PAPER

CrossMark
click for updates

Rice oil as a green source of capping ligands for GdF₃ nanocrystals†

M. Banski,* A. Noculak, J. Misiewicz and A. Podhorodecki

A new synthesis route for colloidal GdF$_3$ nanocrystals was proposed *via* a thermolysis of trifluoroacetate salts. Its novelty arises from the application of a commercially available rice oil (being a mixture of natural triglycerides) as the synthesis solvent. Rice oil decomposes at ~254 °C into glycerol and three fatty acids, being a green source of capping ligands. Rapid nucleation with a low concentration of ligands results in monodisperse nanocrystals, while delayed ligand activation results in well-stabilized nanocrystals in the final stage of the synthesis. The nanocrystals show a synthesis time and temperature dependent size (3–11 nm) and shape (spherical and rhombic). We determined a size range (5.6–9.4 nm) in which the nanocrystals show double morphology (spherical and rhombic), while smaller and bigger NCs exist only in a spherical or a rhombic form, respectively. Detailed analysis of the nanocrystal morphology was followed by spectroscopic investigations of their optical properties. We determined a significant influence of a residual oxygen atom and a high surface to volume ratio on the excitation and emission of Eu^{3+} ions. The contribution of the oxygen diminishes at high temperature and/or with prolonged synthesis.

1. Introduction

Considerable interest has been focused on rare earth doped nanocrystals (NCs) due to their interesting optical properties (arising from their 4f electron configuration) and great possibilities for applications ranging from optical and photonic materials for the development of displays, lasers, and lighting devices, to diagnostic tools in biomedicine, especially in the field of optical imaging.[1,2] In comparison with organic dyes and semiconductor quantum dots, rare earth doped NCs show superior chemical and optical properties, like sharp emission peaks in the VIS and NIR ranges, large Stokes shifts, long fluorescence lifetimes, and a high resistance to photobleaching.[3] In addition, their composition-tunable emission, caused by ion–ion interactions,[4–6] allows for filter free multicolor labeling, which makes possible *e.g.* simultaneous observation of different cell components.

An important category of Ln activated materials is lanthanide fluorides (LnF$_3$) which were recognized as highly efficient hosts for luminescent ions, due to their large energy gap (~9.7 eV) and low phonon frequency (~350 cm^{-1}).[7] Moreover, the high ionicity of the rare earth to fluoride results in restricted electron–phonon coupling and a low probability of excited state nonradiative quenching.[8–10]

Among lanthanide fluorides, the GdF$_3$ matrix exhibits a significant advantage when used as a host matrix. This arises from the 4f^7 electronic configuration, resulting in paramagnetic properties of Gd^{3+} and its popular application as a contrast agent in magnetic resonance imaging (MRI).[11] Recently, Dong *et al.* showed that the highest r_1 relaxivity per Gd^{3+} ion (2.33 mM^{-1} s^{-1}) was measured for NCs capped by a thin NaGdF$_4$ shell (*ca.* 0.6 nm thick) and the extra Gd^{3+} containing shell does not contribute to the relaxivity.[12] Earlier studies by Park *et al.* on Gd$_2$O$_3$ NCs showed that an NC diameter of 1.0–2.5 nm is optimal for the maximal r_1 relaxation.[13] In both cases the enhancement of the longitudinal relaxation of the water proton was related to a cooperative induction by the surface Gd^{3+} ions. This suggests that an enhancement of the proton relaxivity per nanoparticle increases with the surface to volume (S/V) ratio.[14,15] Thus, among various morphologies plate-like shape NCs, where the thickness of particles is of the order of a few unit cells and the S/V ratio is high, seem to be a promising candidate for MRI markers providing a high contrast at low marker concentrations.

Several synthetic methods have been used for the preparation of LnF$_3$ nanoparticles. However, the development of the synthesis of LnF$_3$ NCs is mainly focused on new precursors, adjusted synthesis parameters and the incorporation of various lanthanides.[16] In most of the reports, regardless of whether a hot-injection or a heating up approach is used, oleic acid (OA), oleylamine (OAm) and 1-octadecene (ODA) in different combinations constitute high boiling temperature solvents

Department of Experimental Physics, Wroclaw University of Technology,
Wybrzeze Wyspianskiego 27, 50-370 Wroclaw, Poland.
E-mail: mateusz.banski@pwr.edu.pl

and surface ligands.[17,18] Other authors reported trioctylphosphine oxide (TOPO) in NC synthesis.[19,20] However, TOPO and other organic capping agents have been shown to enhance the toxicity of nanoparticles for *in vivo* applications.[21–23]

Environmental protection extorts to search for a green source of solvents and capping ligands to minimize the harmful impact of nanocrystal synthesis and its applications in the environment. Natural oils are an alternative to air-sensitive, toxic and expensive chemicals such as phosphines, thiols and amines. To our knowledge, only a few authors have proposed a synthesis in environmentally friendly olive oil as a reaction solvent;[24–26] however, they added additional ligands to stabilize the NC surface.

In this study, we report the application of rice oil (RO) as a solvent and simultaneously as a green source of capping ligands, which makes the synthesis of GdF_3 NCs low-cost and convenient. In the one-pot approach, gadolinium trifluoroacetate ($GdTFA_3$) was a single source precursor of Gd, and F. We doped GdF_3 nanocrystals with 5% Eu^{3+} ions in order to make them optically active in the visible range. The advantage of Eu^{3+} ions is their characteristic relationship between the optical response and the crystal field,[27] thus, we used them as a crystal field probe. To better understand the proposed synthesis in RO, we evaluated the influence of the synthesis conditions (temperature and time) on the structural and consequently on the optical properties of Eu^{3+} doped GdF_3 NCs.

2. Experimental

2.1 Synthesis of GdF_3:Eu^{3+} nanocrystals

Europium(III) trifluoroacetate trihydrate $Eu(CF_3COO)_3 \cdot 3H_2O$ (98%), gadolinium(III) oxide Gd_2O_3 (powder, 99.9%) and trifluoroacetic acid (99%) were purchased from Sigma-Aldrich. Rice oil (RO) is a commercially available product of Monini. All chemicals were used directly without further purification. Gadolinium(III) trifluoroacetate was prepared from gadolinium oxide and trifluoroacetic acid according to the literature method.[28,29]

A co-thermolysis of trifluoroacetate salts proposed by Yan's group[16] was modified to synthesize GdF_3:Eu^{3+} NCs in a single-step procedure. For this purpose, a mixture of $Gd(CF_3COO)_3$ (237.5 mg, 0.479 mmol) and $Eu(CF_3COO)_3$ (12.5 mg, 0.025 mmol) was dissolved in RO (10 ml) using standard Schlenk line techniques. The mixture was degassed by rigorous stirring and heating at 120 °C under vacuum. After 30 minutes the temperature was rapidly increased (under a nitrogen flow) and the nucleation and growth process started. Five series of NCs were prepared at 235, 255, 275, 295 and 340 °C. At desired temperatures the samples were annealed for 60 minutes and small quantities of the samples were collected every 15 minutes. Finally, the reaction was cooled to 70 °C and an excess of methanol was added to precipitate the NCs. The resulting material was collected by centrifugation and washed several times with methanol to remove organic residuals from the NC solution. The final products were easily dispersed in nonpolar solvents (*e.g.* cyclohexane).

2.2 Structural characterization

A FEI Tecnai G2 20 X-TWIN transmission electron microscope was used to obtain TEM images of the nanoparticles. NCs for the TEM experiments were washed with methanol at least four times to remove excess capping ligands. A dilute cyclohexane solution of NCs was added dropwise on the carbon coated copper grids and left to evaporate. XRD spectra were recorded on a Philips diffractometer supported by the parallel beam optic and CuK_{α_1} radiation source, $\lambda = 0.15406$ nm.

2.3 Optical characterization

Photon Technology International Inc. systems, equipped with *e.g.* a flash xenon lamp and a strobe detector both coupled with monochromators, were used to observe PLE and PL spectra, and the PL decays. The absorption spectra were measured on a JASCO V-570 spectrophotometer.

Infrared absorption spectra were recorded on a FTIR spectrometer (Nicolet iS10 from Thermo Fisher Scientific) equipped with an attenuated total reflectance sample holder (ATR). For every measurement a few drops of sample were deposited at the ATR crystal. To avoid sample contamination, the ATR crystal was carefully cleaned twice with cyclohexane followed by acetone and dried before the next sample deposition.

3. Results and discussion

3.1 Rice oil composition

RO is a commercially available natural glyceride, which contains unsaturated acids: oleic (41.0%); linolic (36.7%); and saturated acids: myristic (0.3%), palmitic (12.3%), stearic (1.8%), arachidic (0.5%), lignoceric (0.4%) and 4.6% unsaponifiable acid, mostly sterols (25%).[30] The generally accepted smoke point of RO is at ∼254 °C; however, due to a mixture of various acids in glycerides, its experimental determination *via* DSC is imperfect. On the other hand, we measured a DSC plot of glyceryl trioleate, which is the main component of RO, and we determined its smoke point at 204 °C (Fig. S1, ESI†). We postulate that below the smoke point RO plays the role of a non-coordinating organic solvent and at higher temperature, when RO decomposes into glycerol and fatty acids, its coordinating properties are activated.

3.2 Structural characterization

The lanthanide fluorides (LnF_3) crystallize in trigonal and orthorhombic phases. The former is more favorable for lighter lanthanides and the latter is preferred for heavier Ln.[31] The GdF_3 and EuF_3 lie in the intermediate range and both trigonal ($P\bar{3}c1$) and orthorhombic ($Pnma$) crystal phases are possible.[32] The lattice energy (LE) is equal to 5108 kJ mol^{-1} and 5122 kJ mol^{-1} for the trigonal and orthorhombic phases, respectively.[32] The small LE difference stimulates crystal dimorphism. Thus, despite thermodynamically stable GdF_3 bulk materials exhibiting a single orthorhombic phase, both phases should be considered in the case of small-sized GdF_3:Eu^{3+} NCs, where the surface energy plays a critical role.[32]
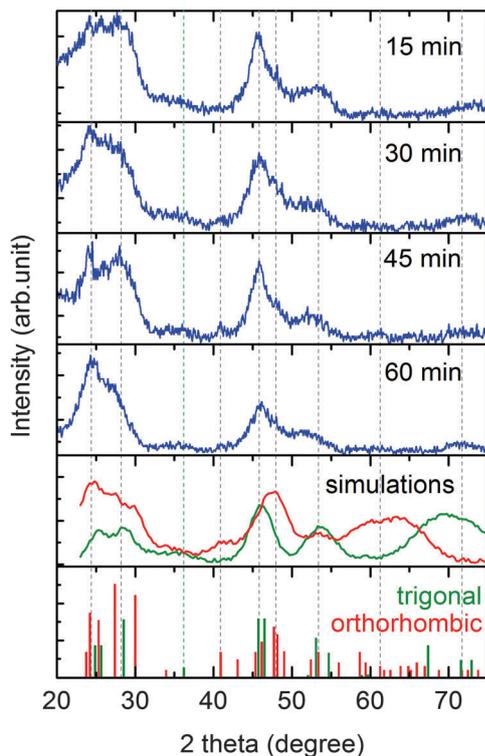
Fig. 1 XRD spectra of GdF$_3$ NCs prepared at various synthesis times for samples prepared at 340 °C. The diffraction peak positions of the orthorhombic (GdF$_3$, PDF no: 12-0788) and trigonal (SmF$_3$, PDF no: 05-0563) phases as well as simulated XRD spectra of 3.5 nm spherical NCs are shown for reference.

At first, we evaluated the influence of the synthesis time on the crystal phase of GdF$_3$ NCs. Fig. 1 shows the XRD patterns of GdF$_3$ NCs prepared at 340 °C for 15, 30, 45 and 60 minutes and the suitable XRD reference of the trigonal and orthorhombic phases. Despite the presence of diffraction peaks for all investigated samples, the significant broadening of the peaks and the overlapping of multiple peaks hamper the unequivocal recognition of the crystal phase. To better evaluate the crystal phase of the synthesized NCs we simulated XRD spectra of ∼3.5 nm spherical NCs of the trigonal and orthorhombic phases (Fig. 1). Based on the comparison between the simulated and measured peaks, it can be seen that the diffraction peaks above 58 degrees are hardly visible; the two peaks of the trigonal phase at ∼46 and ∼53 degrees correspond well to NCs after 15 minutes of synthesis. During the synthesis these peaks do not disappear, but are broadened and slightly shifted (e.g. 53.3° → 51.4°); this is what we recognize as the formation of the orthorhombic phase. This is in agreement with the analysis of the peaks at 20–35 degrees. With the increase in synthesis time, the peak at ∼24.4° increases, while the peak at ∼28.6° decreases. These peaks are related to the orthorhombic and trigonal phases, respectively. Thus, we conclude that during the as-discussed synthesis of GdF$_3$ NCs at 340 °C the NCs are initially in the trigonal phase and evolve with time to the orthorhombic phase.

Lorbeer et al. have already shown that the crystal phase of sub-10 nm GdF$_3$ NCs can change from the orthorhombic to trigonal phase depending on the synthesis conditions.[33] The XRD results are supported by TEM imaging of GdF$_3$ NCs synthesized at various synthesis times (Fig. 2a–d). The TEM images present monodisperse and well separated GdF$_3$ NCs, which in the initial step (15 minutes) are mostly in the spherical form. The average diameter of these NCs was calculated to be ∼6.1 nm (Fig. 2e). When the synthesis time is elongated, the rhombic fraction of the NCs begins to dominate in the ensemble over spherical NCs. The well-defined shape, with sharp edges and corners, suggests that the prolonged synthesis at 340 °C is associated with a thermodynamically driven growth. The confirmation can be found in the size distributions of the NCs (Fig. 2e–h), where

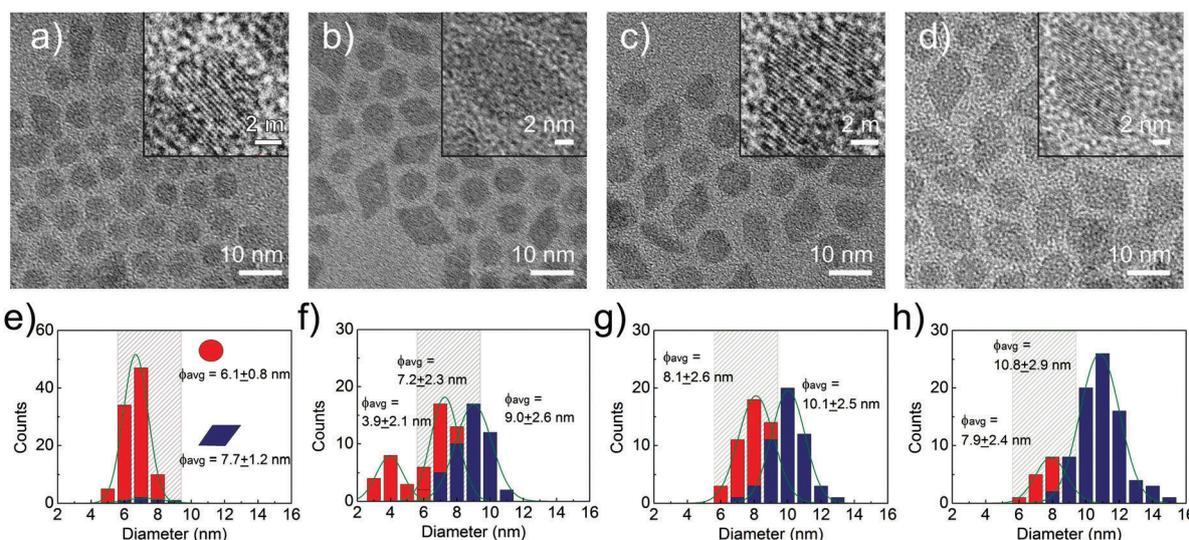**Fig. 2** TEM images and size distributions of the growth of GdF$_3$ NCs at 340 °C for 15 min (a and e), 30 min (b and f), 45 min (c and g) and 60 min (d and h). Insets in TEM images show magnified single NCs with lattice fringes. The shaded area in size distribution corresponds to the size range where the double morphology of NCs occurs.

two groups (spherical and rhombs) of nanocrystals can be distinguished. For a synthesis time of 15 minutes the average diameter of the spherical NCs and the average edge length of the rhombic NCs were 6.1 and 7.7 nm, respectively. After 30 minutes of synthesis, the number of spherical NCs was significantly reduced and many of them were smaller ($\sim$3.9 nm). In contrast, the average size of the rhombic NCs increased. We proposed that a thermodynamically driven Ostwald ripening process was responsible for the dissolution of smaller spherical NCs and the growth of the rhombic ones. When this process was continued, the length of the rhombic NCs was 10.1 nm and 10.8 nm for 45 and 60 minutes, respectively. Simultaneously, the fraction of spherical NCs was found to be decreasing continuously. After 120 minutes of the synthesis only rhombic NCs remained (Fig. S2, ESI†). Interestingly, only spherical NCs smaller than 5.6 nm have been dissolved. The spherical NCs of size in the range 5.6–9.4 nm remained in the ensemble even after 60 minutes of synthesis. On the other hand, there were no rhombic NCs smaller than 5.6 nm and their size was continuously increasing with synthesis time. Thus, the GdF_3 NCs in the size range 5.6–9.4 nm show a double morphology (spherical and rhombic), while smaller and bigger NCs exist only in the spherical and rhombic forms, respectively.

In order to further examine the crystal phase of the NCs, we analyzed the lattice-fringes based on high-resolution TEM images, which are presented in the insets of Fig. 2a–d. These images present a single NC with a well-defined crystal lattice. Based on that, we calculated the lattice spacing to be close to 0.35 nm for all the samples, which is characteristic of the (010) plane of the orthorhombic phase.[16] On the other hand, the interplanar spacing of the (0002) layers in the trigonal phase is $\sim$0.36 nm. Thus, combining TEM and XRD results, we conclude that after 60 minutes at 340 °C most NCs crystallize in the orthorhombic phase and have the rhombic shape. However, at the earlier stages of the synthesis, the NCs are in the trigonal phase and we cannot exclude that the shape transformation is associated with the crystal phase transition.

In order to confirm the role of high temperature in the shape transition of NCs, we evaluated the influence of temperature on the growth of GdF_3 NCs. TEM images of the GdF_3 NCs synthesized at various temperatures (Fig. S3, ESI†) show increasing number of spherical particles in the NC ensemble when the temperature is lowered. The NCs synthesized for 60 minutes at 340 °C are mainly of the rhombic shape, while for the sample synthesized at 255 °C spherical NCs with small admixtures of elongated particles are present in the images. Most probably, the elongated shape comes from an edge of flat, rhombic nanoparticles being self-organized into a ladder-like pattern. The morphological dualism, which depends on the synthesis temperature, seems to be thermodynamically driven.

Fig. S4 (ESI†) shows the XRD patterns of GdF_3 NCs synthesized in the temperature range of 235 to 340 °C. No diffraction pattern was found for the sample prepared at the lowest temperature (235 °C). For the samples synthesized at higher temperatures (255–340 °C) the diffraction peaks are clearly present. For spherical NCs synthesized for 60 minutes at 255 °C (Fig. S4, ESI†) and those synthesized for 15 minutes at

340 °C XRD (Fig. 1), their spectra were found to be similar. Then, a similar evolution in the XRD patterns was induced by both a higher synthesis temperature and a longer synthesis time at 340 °C when the NCs transformed from the spherical to rhombic shape.

The ladder-like pattern, like the one presented in Fig. S3a and b (ESI†), is formed in the ensemble of nanoparticles when their surface is effectively covered with a ligand layer.[34] The distance between the NCs in the "ladder" was calculated to be in the range of 3.5–4.0 nm. This is in good agreement with a doubled length of a long-chain fatty acid molecule.[35] The assembly effect is strongly related to the minimization of energy and it is achieved through hydrophobic interactions of the surface ligands of the nanoparticles which are located at the largest facets.[36] This is important evidence of efficient surface passivation of NCs by ligands from RO.

3.3 FT-IR ligand analysis

The successful synthesis of NCs *via* wet chemistry methods requires coordinating ligands attached to the nanoparticle's surface to stabilize their dispersion in colloidal solution. Using FT-IR spectroscopy we determined the ligands related to characteristic functional groups, which are located at the surface of the GdF_3 nanocrystals due to the synthesis in rice oil. In Fig. 3 FT-IR spectra of rice oil (RO), glyceryl trioleate (GTO), oleic acid (OA),
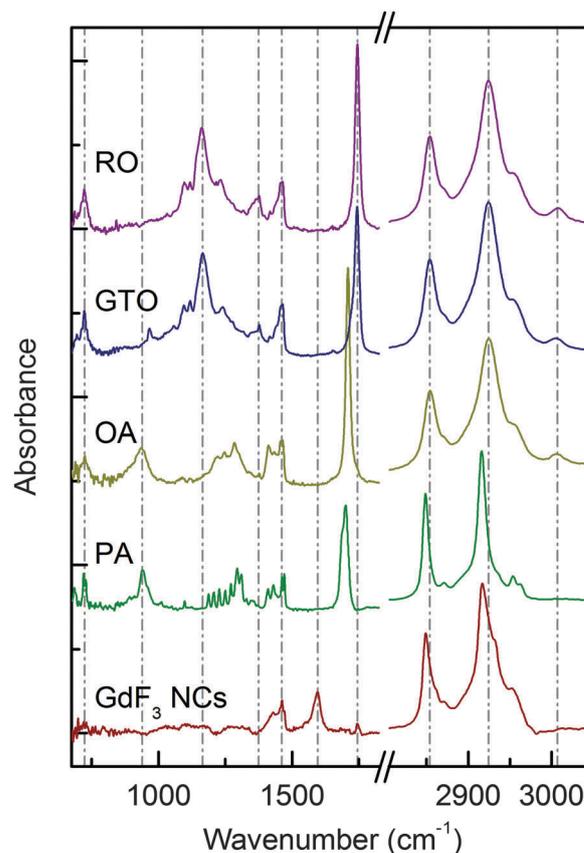

Fig. 3 FT-IR spectra of rice oil (RO), glyceryl trioleate (GTO), oleic acid (OA), palmitic acid (PA) and GdF_3 NCs synthesized in RO at 340 °C.
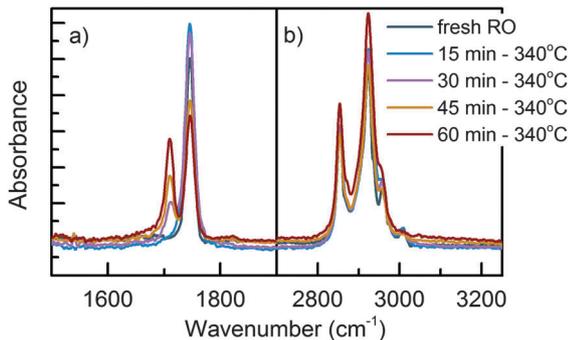
Fig. 4 FT-IR spectra of rice oil (RO) heated at 340 °C for various times.

palmitic acid (PA) and synthesized GdF_3 NCs are shown. The absorption band at ~ 1709 cm^{-1} is related to the C=O stretching mode of free carboxylic acid groups (–COOH) and was observed for OA and PA only. For GTO carboxyl groups from aliphatic esters (–COOR) were observed as a band at 1745 cm^{-1}, which arises from the C=O stretching mode. In the spectra of RO the band at 1745 cm^{-1} is very intense, whereas the one at 1705 cm^{-1} is absent. Thus, the commercially available RO contains mostly triglycerides and free carboxylic acids were not detected. Moreover, the FT-IR spectra in Fig. 4a revealed that heat treatment of RO causes an increase of the carboxylic acid concentration while the concentration of triglycerides decreases in the synthesis solution.

For GdF_3 NCs the bands at 1745 and 1705 cm^{-1} disappear and a new band centered at 1596 cm^{-1} appears providing direct evidence of the attachment of carboxylic acids to the nanocrystal surface.

A weak band observed at 1655 cm^{-1} was assigned to the C=C stretching mode of the unsaturated hydrocarbon chain. Moreover, a band at 3007 cm^{-1} arises from C–H stretching vibrations in –HC=CH–. These bands are present in the spectra of OA and GTO as expected. However, they are also visible for RO with comparable intensity. This confirms that many of the triglycerides from RO contain unsaturated acids. However, this band is absent in the spectrum of GdF_3 NCs. Moreover, for OA, GTO and RO, two intensive bands centered at 2854 cm^{-1} and 2925 cm^{-1} are observed. They arise from symmetric and asymmetric CH$_2$ stretching modes, respectively. These bands are slightly shifted for PA (2848 cm^{-1}, 2916 cm^{-1}), which is due to interaction between saturated hydrocarbon chains.[37] For GdF_3 NCs the positions of the –CH$_2$ stretching modes agree with those of PA. Based on the above results we proposed that despite triglycerides of unsaturated acids being the main component of RO, and the fact that a high temperature treatment of RO does not cause saturation of unsaturated acids (Fig. 4b), the ligands at the NC surface are mostly the anions of saturated fatty acids originating from minor saturated triglycerides of RO.

3.4 Optical properties

The interesting optical properties of the investigated NCs arise from the Eu^{3+} ion dopant. Based on the EDX spectra, the Eu^{3+} doping level of the GdF_3 host is around $\sim 6\%$ (Fig. S5, ESI†).
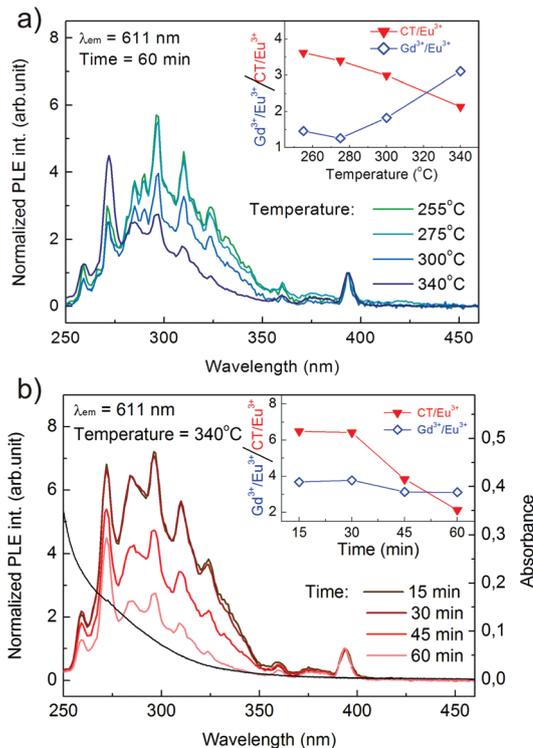

Fig. 5 PLE spectra of GdF_3:Eu^{3+} NCs synthesized at (a) various temperatures for 60 minutes and (b) with various synthesis times at 340 °C. All spectra were normalized to the intensity of direct Eu^{3+} excitation at 395 nm. Absorption spectra of GdF_3:Eu^{3+} synthesized at 340 °C for 60 min are also indicated (black line). The insets show the intensity ratios of indirect excitation via Gd^{3+} and CT states in relation to direct Eu^{3+} excitation, Gd^{3+}/Eu^{3+}, CT/Eu^{3+} respectively.

To understand the mechanism of Eu^{3+} ion excitation in GdF_3, matrix photoluminescence excitation (PLE) spectra were recorded (Fig. 5). The Eu^{3+} emission was excited by the range of excitation bands related to the intra-orbital 4f–4f transitions. The most efficient direct excitation of Eu^{3+} ions is due to the $^7F_0$–$^5L_6$ transition at a 395 nm wavelength. An indirect excitation is possible for the 272 nm wavelength, for which photons are absorbed by Gd^{3+} due to the $^8S_{7/2}$–^6I_J transition, then, the energy is nonradiatively transferred to Eu^{3+} ions from which a radiative recombination may occur. In the insets of Fig. 5a, the intensity ratio of the Gd^{3+}/Eu^{3+} excitation bands is shown and it significantly increases for the synthesis at temperatures higher than 275 °C. Moreover, at 340 °C the Gd^{3+}/Eu^{3+} intensity ratio is roughly independent of the synthesis time (inset of Fig. 5b). This means that the temperature of the synthesis, not the growth time, influences the energy migration from Gd^{3+} to Eu^{3+} ions.

The above-discussed Gd^{3+} and Eu^{3+} excitation peaks lie on a broad band centered at ~ 295 nm. This band is common to all the prepared samples. Several different origins of the absorption band in the UV range are possible for the lanthanide doped fluoride nanocrystals, e.g. defect states, ligands, and charge transfer transition.[38–42] We proposed that, in the case of the discussed GdF_3:Eu^{3+} NCs, the broad band in the UV originates from the excitation of Eu^{3+} ions via a CT transition involving

Eu^{3+} ions and oxygen (substitution and/or interstitial atoms) in the GdF$_3$ matrix. This assumption is based on the spectral broadening and the relatively high efficiency of Eu^{3+} excitation *via* this band. This band is hardly visible in the absorption spectrum (Fig. 5b) for which a ligand absorption is the main contributor in the UV but is clearly present in the PLE spectra. The insets of Fig. 5 show the integrated intensity ratio of CT to direct Eu^{3+} excitation bands (CT/Eu^{3+}). The ratio decreases with the increase in synthesis temperature, as well as with prolonged synthesis time. We interpreted this as a reduction of the number of oxygen atoms in the monocrystalline matrix. Fig. 6 shows the PL spectra of GdF$_3$:Eu^{3+} NCs prepared for 60 minutes at various temperatures (a–d) and at 340 °C for various synthesis times (e–h). For each sample, the PL spectra were recorded using two excitation wavelengths (λ_{exc}) 395 and 295 nm, which are related to Eu^{3+} excitation *via* direct f–f ($^{7}F_0$–$^{5}L_6$) and CT mediated

transitions, respectively. The two main emission peaks of Eu^{3+} ions at 590 nm and 612 nm are related to magnetic dipole (MD–$^{5}D_0$–$^{7}F_1$) and electric dipole (ED–$^{5}D_0$–$^{7}F_2$) transitions, respectively. Independent of the excitation wavelength, the ED transition at 612 nm is very intense compared to the MD transition, which according to the literature is unusual for the orthorhombic as well as trigonal phases of GdF$_3$.[33]

For longer times and/or higher temperatures of the synthesis, when the spherical to rhombic shape transition took place, there was no crucial change in the PL spectra. This is also unusual, since the emission properties are strongly governed by the symmetry of the crystal.

To quantitatively investigate the changes of the Eu^{3+} emission bands, under different synthesis conditions, we determined the ED to MD integrated intensity ratio (ED/MD) which is a sensitive probe of the local crystal field symmetry (Fig. 6i). In the case of direct Eu^{3+} excitation, the ED/MD ratio slightly decreases from 1.2 to 1.0 with increasing synthesis temperature. In the literature, the characteristic ED/MD value for trigonal as well as ortho-rhombic phases is certainly below 1.0.[33] An uncommonly high ED/MD ratio agrees with the prior suggestion that oxygen is incorporated into our GdF$_3$ NCs and influences the optical response of Eu^{3+} ions by the modification of their local crystal field.

The additional information can be extracted from the PL spectra where the CT transition at λ_{exc} = 295 nm is used to excite NCs. In this case, the ED/MD ratio is equal to 1.52 and is roughly constant for all investigated samples. In the literature, an exceptionally high ED/MD ratio was reported for very narrow EuOF nanowires with a high surface to volume ratio.[43] In our case we suggest that the CT transition excites Eu^{3+} located at low symmetry sites, close to oxygen at the surface of the NCs. These surface Eu^{3+} ions contribute to the high ED/MD ratio.[44] This is in agreement with the evolution of the CT/Eu^{3+} excitation intensity ratio (observed for PLE in Fig. 5). For higher tem-peratures and longer synthesis times, when the shape transition of NCs takes places, the CT/Eu^{3+} ratio decreases with the surface to volume ratio.

4. Conclusions

Herein we report a successful synthesis of sub-10 nm GdF$_3$ nanocrystals using rice oil as a solvent and a green source of capping ligands. Particularly, saturated acids coming from the decomposition of a triglyceride mixture were found to effi-ciently passivate the NC surface. After 60 minutes at 340 °C GdF$_3$ NCs crystallized in the orthorhombic phase and have a rhombic shape. For a lower synthesis temperature and shorter synthesis time a mixture of spherical and/or rhombic shapes was present in the NC ensemble. We associated the shape transition with thermodynamically driven annealing when the number of oxygen atoms in the crystal lattice is reduced. Furthermore, the electric dipole transition of Eu^{3+} ions is significantly more probable in all synthesized GdF$_3$:Eu^{3+} NCs as compared to its bulk form. This is probably due to the oxygen atoms at the NC surface, which distort the crystal field

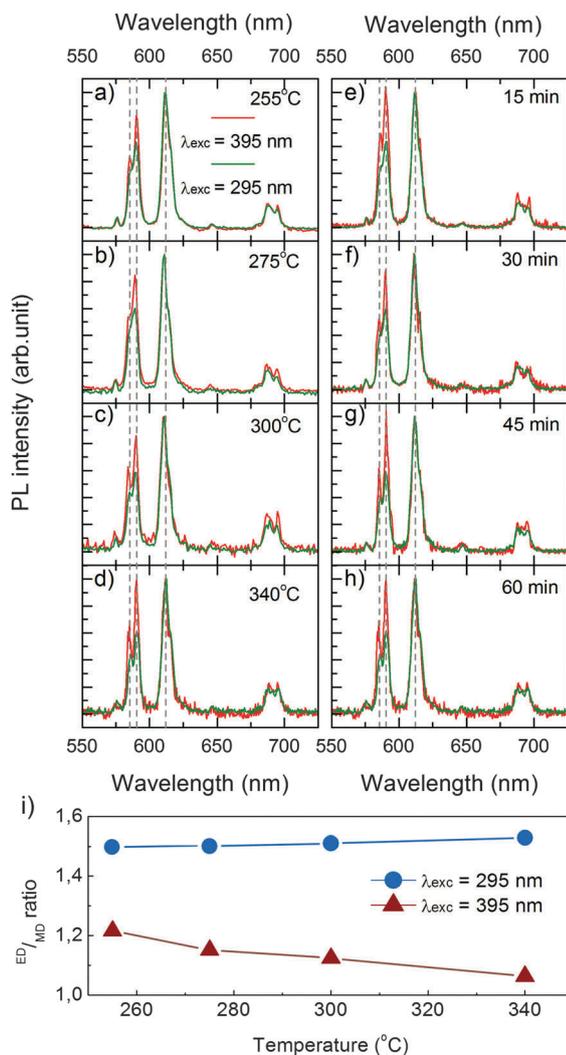**Fig. 6** PL spectra of GdF$_3$:Eu^{3+} NCs synthesized (a–d) at various tem-peratures for 60 minutes and (e–h) at 340 °C for various synthesis times. Two excitation pathways were examined: direct, due to 4f–4f transition (λ_{exc} = 395 nm), and indirect, due to CT (λ_{exc} = 295 nm). The ED/MD ratios for GdF$_3$:Eu^{3+} NCs prepared at various synthesis temperatures (i).

symmetry and modify the Eu^{3+} emission. Due to the high surface to volume ratio, surface Eu^{3+} ions contribute significantly to the PL spectra. Plate-like rhombic GdF_3:Eu^3 NCs are promising structures for a dual-mode bio-marker due to intensive Eu^{3+} photoluminescence and a high number of surface Gd^{3+} ions contributing to a very high r_1 relaxivity.

Acknowledgements

References

1 L. M. Maestro, E. M. Rodriguez, F. Vetrone, R. Naccache, H. L. Ramirez, D. Jaque, J. A. Capobianco and J. G. Solé, *Opt. Express*, 2010, **18**, 23544–23553.

2 F. Vetrone and J. A. Capobianco, *Int. J. Nanotechnol.*, 2008, **5**, 1306.

3 A. M. Coto-García, E. Sotelo-González, M. T. Fernández-Argüelles, R. Pereiro, J. M. Costa-Fernández and A. Sanz-Medel, *Anal. Bioanal. Chem.*, 2011, **399**, 29–42.

4 A. Podhorodecki, M. Banski, J. Misiewicz, M. Afzaal, P. O'Brien, D. Cha and X. Wang, *J. Mater. Chem.*, 2012, **22**, 5356–5361.

5 M. Banski, A. Podhorodecki, J. Misiewicz, M. Afzaal, A. L. Abdelhady and P. O'Brien, *J. Mater. Chem. C*, 2012, **1**, 801–807.

6 A. Podhorodecki, M. Banski, A. Noculak, B. Sojka, G. Pawlik and J. Misiewicz, *Nanoscale*, 2013, **5**, 429–436.

7 H. Wiemhofer, *Solid State Ionics*, 1990, 433–439.

8 E. Bovero and F. C. J. M. vanVeggel, *J. Phys. Chem. C*, 2007, **111**, 4529–4534.

9 S. Sivakumar, F. C. J. M. van Veggel and M. Raudsepp, *J. Am. Chem. Soc.*, 2005, **127**, 12464–12465.

10 M. J. Weber, *Phys. Rev.*, 1967, **157**, 262–272.

11 M. M. Hüber, A. B. Staubli, K. Kustedjo, M. H. Gray, J. Shih, S. E. Fraser, R. E. Jacobs and T. J. Meade, *Bioconjugate Chem.*, 1998, **9**, 242–249.

12 C. Dong, A. Korinek, B. Blasiak, B. Tomanek and F. C. J. M. van Veggel, *Chem. Mater.*, 2012, **24**, 1297–1305.

13 J. Y. Park, M. J. Baek, E. S. Choi, S. Woo, J. H. Kim, T. J. Kim, J. C. Jung, K. S. Chae, Y. Chang and G. H. Lee, *ACS Nano*, 2009, **3**, 3663–3669.

14 Y. Li, T. Chen, W. Tan and D. R. Talham, *Langmuir*, 2014, **30**, 5873–5879.

15 N. J. J. Johnson, W. Oakden, G. J. Stanisz, R. Scott Prosser and F. C. J. M. van Veggel, *Chem. Mater.*, 2011, **23**, 3714–3722.

16 X. Sun, Y.-W. Zhang, Y.-P. Du, Z.-G. Yan, R. Si, L.-P. You and C.-H. Yan, *Chem. Weinh. Bergstr. Ger.*, 2007, **13**, 2320–2332.

17 A. D. Ostrowski, E. M. Chan, D. J. Gargas, E. M. Katz, G. Han, P. J. Schuck, D. J. Milliron and B. E. Cohen, *ACS Nano*, 2012, **6**, 2686–2692.

18 X. Teng, Y. Zhu, W. Wei, S. Wang, J. Huang, R. Naccache, W. Hu, A. I. Y. Tok, Y. Han, Q. Zhang, Q. Fan, W. Huang, J. A. Capobianco and L. Huang, *J. Am. Chem. Soc.*, 2012, **134**, 8340–8343.

19 X. D. Luo, U. Farva, N. T. N. Truong, K. S. Son, P. S. Liu, C. Adachi and C. Park, *J. Cryst. Growth*, 2012, **339**, 22–30.

20 J. Ma, *J. Wuhan Univ. Technol., Mater. Sci. Ed.*, 2011, **26**, 611–614.

21 J. Aldana, Y. A. Wang and X. Peng, *J. Am. Chem. Soc.*, 2001, **123**, 8844–8850.

22 A. M. Derfus, W. C. W. Chan and N. B. Sangeeta, *Nano Lett.*, 2004, **4**, 11–18.

23 L. P. A. Cornacchio and N. D. Jones, *J. Mater. Chem.*, 2006, **16**, 1171–1177.

24 J. Akhtar, M. A. Malik, P. O'Brien and N. Revaprasadu, *Mater. Lett.*, 2012, **77**, 78–81.

25 S. Sapra, A. L. Rogach and J. Feldmann, *J. Mater. Chem.*, 2006, **16**, 3391–3395.

26 N. Xiao, Q. Dai, Y. Wang, J. Ning, B. Liu, G. Zou and B. Zou, *J. Hazard. Mater.*, 2012, **211–212**, 62–67.

27 N. Hildebrandt and H.-G. Lohmannsroben, *Curr. Chem. Biol.*, 2007, **1**, 167–186.

28 H.-X. Mai, Y.-W. Zhang, R. Si, Z.-G. Yan, L. Sun, L.-P. You and C.-H. Yan, *J. Am. Chem. Soc.*, 2006, **128**, 6426–6436.

29 J. E. Roberts, *J. Am. Chem. Soc.*, 1961, **83**, 1087–1088.

30 G. S. Jamieson, *J. Oil Fat Ind.*, 1926, **3**, 256–261.

31 X. Ye, J. Chen, M. Engel, J. A. Millan, W. Li, L. Qi, G. Xing, J. E. Collins, C. R. Kagan, J. Li, S. C. Glotzer and C. B. Murray, *Nat. Chem.*, 2013, **5**, 466–473.

32 C. Dong, M. Raudsepp and F. C. J. M. van Veggel, *J. Phys. Chem. C*, 2009, **113**, 472–478.

33 C. Lorbeer, J. Cybinska and A.-V. Mudring, *J. Mater. Chem. C*, 2014, **2**, 1862–1868.

34 A. A. L. Pavel and P. Fedorov, *J. Fluorine Chem.*, 2011, **132**, 1012–1039.

35 C. Lopez, C. Bourgaux, P. Lesieur, A. Riaublanc and M. Ollivon, *Chem. Phys. Lipids*, 2006, **144**, 17–33.

36 H. Wang and T. Nann, *Nanoscale Res. Lett.*, 2011, **6**, 267.

37 I. W. L. Ian and R. Hill, *J. Chem. Phys.*, 1979, **70**, 842–851.

38 M. Banski, M. Afzaal, A. Podhorodecki, J. Misiewicz, A. L. Abdelhady and P. O'Brien, *J. Nanopart. Res.*, 2012, **14**, 1228.

39 R. X. Yan and Y. D. Li, *Adv. Funct. Mater.*, 2005, **15**, 763–770.

40 M. Banski, A. Podhorodecki and J. Misiewicz, *Phys. Chem. Chem. Phys.*, 2013, **15**, 19232–19241.

41 M. Banski, M. Afzaal, D. Cha, X. Wang, H. Tan, J. Misiewicz and A. Podhorodecki, *J. Mater. Chem. C*, 2014, **2**, 9911–9917.

42 W. Yu, X. Wang, N. Chen, G. Du and W. Gui, *CrystEngComm*, 2014, **16**, 3214–3221.

43 Y.-P. Du, Y.-W. Zhang, Z.-G. Yan, L.-D. Sun and C.-H. Yan, *J. Am. Chem. Soc.*, 2009, **131**, 16364–16365.

44 A. Podhorodecki, N. V. Gaponenko, M. Banski, M. V. Rudenko, L. S. Khoroshko, A. Sieradzki and J. Misiewicz, *Opt. Mater.*, 2012, **34**, 1570–1574.